OPEN ACCESS
IOP PUBLISHING
SCIENCE AND TECHNOLOGY OF ADVANCED MATERIALS
Sci. Technol. Adv. Mater. **14** (2013) 014208 (9pp)
doi:10.1088/1468-6996/14/1/014208

Microstructure and cleavage in lath martensitic steels

John W Morris Jr[1], Chris Kinney[1], Ken Pytlewski[1] and Y Adachi[2]

[1] Department of Materials Science and Engineering, University of California, Berkeley, CA 94620, USA
[2] Department of Mechanical Engineering, Kagoshima University, Kagoshima, Japan

E-mail: jwmorris@berkeley.edu

Received 8 August 2012
Accepted for publication 27 December 2012
Published 20 March 2013
Online at stacks.iop.org/STAM/14/014208

Abstract
In this paper we discuss the microstructure of lath martensitic steels and the mechanisms by which it controls cleavage fracture. The specific experimental example is a 9Ni (9 wt% Ni) steel annealed to have a large prior austenite grain size, then examined and tested in the as-quenched condition to produce a relatively coarse lath martensite. The microstructure is shown to approximate the recently identified 'classic' lath martensite structure: prior austenite grains are divided into packets, packets are subdivided into blocks, and blocks contain interleaved laths whose variants are the two Kurjumov–Sachs relations that share the same Bain axis of the transformation. When the steel is fractured in brittle cleavage, the laths in the block share {100} cleavage planes and cleave as a unit. However, cleavage cracks deflect or blunt at the boundaries between blocks with different Bain axes. It follows that, as predicted, the block size governs the effective grain size for cleavage.

Keywords: lath martensitic steels, cleavage, microstructure, fracture

1. Introduction

The problem of the ductile–brittle transition in structural metals has been known in some form for centuries, and was addressed scientifically as far back as the 19th century [1]. While all of the brittle fracture phenomena in structural materials are interesting and important, the brittle transition to cleavage fracture in dislocated-lath martensitic steels is of particular interest, for at least two reasons.

Firstly, the ductile–brittle transition in lath martensitic steels has important technological implications. The most prominent of the high-strength steels now used or proposed for low-temperature, arctic or cryogenic service are lath martensitic steels, ranging from classic alloys like 4340 to cryogenic steels such as 9Ni steel and the cost-effective Fe–Mn grades now under development to the most modern high strength/high toughness alloys such as Aermet 100 and AF 1410. The transition to brittle cleavage fracture is particularly important since cleavage is the 'inherent' brittle fracture mode in materials with the bcc structure [1, 2].

Secondly, prior research on the microstructure and toughness of lath martensitic steels has produced a semi-quantitative understanding of the transition from ductile to cleavage fracture that is becoming widely accepted and is increasingly driving the metallurgy of high strength steels. Moreover, the probative research tools required to map the complex crystallographic relations in lath martensites are now available in instrumentation that can be used effectively by non-specialists. It is now possible to discuss the fundamental mechanisms of the ductile–brittle transition in dislocated martensite with some real confidence that its features are understood [2–4].

In this paper we shall discuss the microstructure of lath martensitic steels and show how it influences the nature and pattern of cleavage fracture. The experimental example is a coarse-grained Fe–9Ni steel characterized by electron backscatter diffraction.

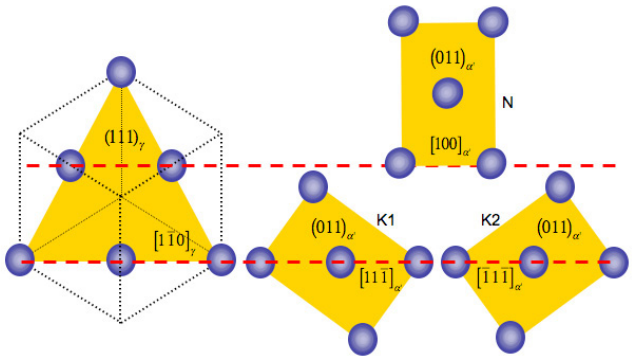

Figure 1. Illustration of the two KS relations and the NW relation that are obtained by aligning the $\langle 110\rangle_\alpha$, and $\langle 100\rangle_\alpha$, directions in the $(011)_\alpha$, plane with the $[1\bar{1}0]_\gamma$ direction in the $(111)_\gamma$ plane. The three variants are examples of each of the three Bain variants.

Table 1. The nine orientations for the planar match $(111)_\gamma||(011)_\alpha$.

Variant*	bcc direction	fcc direction	Maki [6]
K1X	$[11\bar{1}]$	$[1\bar{1}0]$	V5
K1Y	$[11\bar{1}]$	$[01\bar{1}]$	V3
K1Z	$[11\bar{1}]$	$[10\bar{1}]$	V1
K2X	$[\bar{1}1\bar{1}]$	$[10\bar{1}]$	V2
K2Y	$[\bar{1}1\bar{1}]$	$[1\bar{1}0]$	V6
K2Z	$[\bar{1}1\bar{1}]$	$[01\bar{1}]$	V4
NX	[100]	$[01\bar{1}]$	–
NY	[100]	$[10\bar{1}]$	–
NZ	[100]	$[1\bar{1}0]$	–

* *K1* and *K2* label the two KS relations, *N* labels the *NW* relation; *X*, *Y*, *Z* denote the Bain axis. The notation used here is adapted from that in [9].

2. The microstructure of lath martensitic steel

2.1. The KS relation and its variants

While the basic microstructure of lath martensitic steel has long been known [4, 5], its details were clarified significantly by recent research that used methods such as electron backscatter diffraction (EBSD) to characterize the relevant elements. The modern phenomenological view of the lath martensite microstructure is presented, for example, in recent papers by Maki, Morito, Furuhara and co-workers [6–8]. Key features of the martensitic microstructure have also been found in Bainitic and ferritic steels, which broadens the applicability of the results.

In a typical dislocated martensite, the martensite laths have a Kurjumov–Sachs (KS) crystallographic relation to the parent austenite. The KS relation minimizes energy by aligning the phases so that they share a close-packed plane and close-packed direction. The crystallography of this fit is illustrated in figure 1, which sets the close packed $(011)_\alpha$ plane of the bcc martensite parallel to the $(111)_\gamma$ plane of the fcc austenite, and then shows three possible ways of matching low-index directions of the bcc crystal to the close-packed $[1\bar{1}0]$ direction of fcc. Two of these, labeled K1 and K2 in the figure, have close-packed $\langle 111\rangle_\alpha$ directions aligned with $[1\bar{1}0]_\gamma$, and satisfy the KS relations. The third sets $[100]_\alpha$ parallel to $[1\bar{1}0]_\gamma$, giving the alternate Nishiyama–Wasserman (NW) relation [9].

There are three possible choices for the close-packed $\langle 110\rangle_\gamma$ direction in the $(111)_\gamma$ plane and, hence, a total of six KS relations and three NW relations for the pairing $(111)_\gamma||(011)_\alpha$. Since there are four independent choices for the close-packed $\{111\}_\gamma$ reference plane, there are a total of 24 independent KS orientations and 12 independent NW orientations for martensite laths produced by the transformation of a given crystal grain of austenite. These define the possible variants of the martensite laths. While the NW relation is occasionally observed, martensite laths are usually KS-related to the parent austenite, so we shall focus on them.

To describe the nature and consequence of the pattern of the variants that actually appear in a lath martensitic steel we need a nomenclature that distinguishes them. Two methods of labeling have been proposed. The labeling proposed by Maki and co-workers [5–8] simply numbers the variants sequentially, V1, ..., V24, with the numbers divided in sets of six so that a given sequential set, for example, V1, ..., V6, labels the variants that correspond to a particular one of the four pairings $\{111\}_\gamma||\{110\}_\alpha$.

For reasons that will become clear below, we prefer the 'Bain-variant' notation that was proposed by Guo *et al* [9]. To motivate this notation note that the martensite variant can be obtained from the austenite parent in two steps: first, the austenite crystal is compressed along one of the $\langle 100\rangle_\gamma$ cube axes and expanded in the perpendicular planes until it becomes bcc. The strain required to accomplish this is the well-known 'Bain strain'. The transformed crystal is then rotated and slightly sheared to match the close-packed planes and the crystal directions required by the KS or NW relation. The result is a crystal that is both strained and rotated. But only the strain introduces elastic energy; a rigid rotation leaves the energy invariant. Specific computation of the transformation strains required to create the various martensite variants in their final crystallographic relation to the parent austenite shows that the strain is due almost entirely to the Bain strain; the supplementary shear is small and relatively inconsequential. For pure iron, the transformation strains associated with the three Bain variants in figure 1 are [9]

$$E_{K1X} = \begin{bmatrix} -0.196 & -0.0002 & -0.0002 \\ -0.0002 & 0.137 & 0.0003 \\ -0.0002 & 0.0003 & 0.137 \end{bmatrix},$$
$$E_{K2Y} = \begin{bmatrix} 0.137 & -0.0002 & 0.0003 \\ -0.0002 & -0.196 & -0.0002 \\ 0.0003 & -0.0002 & 0.137 \end{bmatrix}, \quad (1)$$
$$E_{NZ} = \begin{bmatrix} 0.137 & -0.0006 & 0.0002 \\ -0.0006 & 0.137 & 0.0002 \\ 0.0002 & 0.0002 & -0.196 \end{bmatrix}.$$

Transformation strains for the other KS and NW variants that are listed in table 1 can be obtained from these by symmetry. Note that the transformation strains are dominated by the diagonal Bain strain.

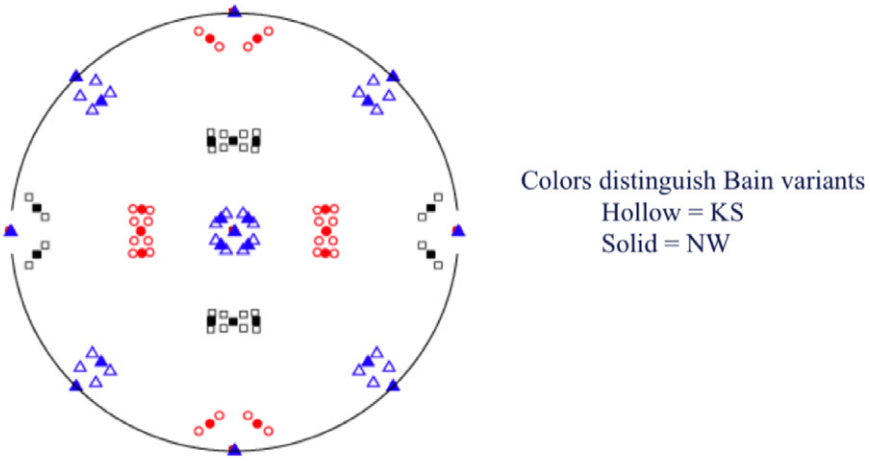

Figure 2. Stereographic projections of the ⟨100⟩ pole figures for the KS and NW variants of martensite derived from a single crystal of austenite. The open symbols are KS variants; the closed symbols are NW variants. The red circles, black squares and green triangles denote the *x*, *y* and *z* Bain variants, respectively.

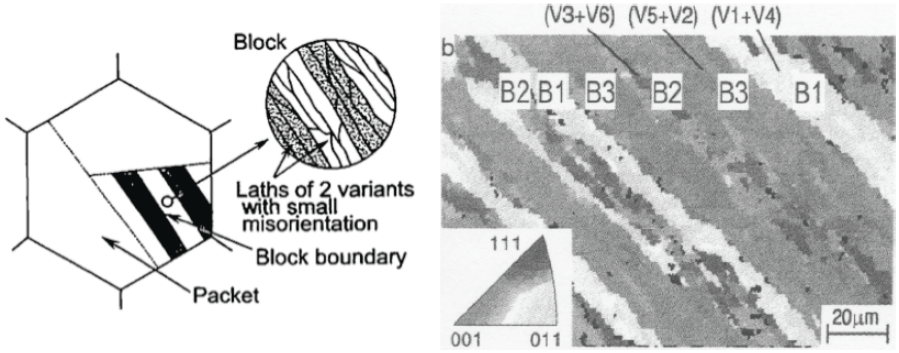

Figure 3. The microstructure of lath martensite developed on quenching a coarse-grained martensite. The prior austenite grain is subdivided into 'packets' that are subdivided into 'blocks' which may contain two sets of interwoven KS-variant laths (from [6]). The left panel is a schematic of the martensitic structure. The right panel is an EBSD map of the alternating block structure, each block composed of two KS variants.

It follows that the most significant feature of a martensite variant is its Bain axis; the cube axis of the austenite that was, in effect, compressed to create it. The Bain axis determines the transformation strain, and also determines the relative orientation of its {100} planes. The 'Bain variant' of a martensite lath can be identified by its image point in a (100) pole figure that plots all of the martensite variants that have KS or NW relations with a given parent austenite crystal. As shown in figure 2, the image points cluster in well-separated groups; the representatives of a given Bain variant have [100] axes that are closely aligned with one another, but rotated significantly with respect to the [100] axes of either of the other Bain variants.

Given that the Bain variant of a lath determines both the geometry of its transformation strain and the alignment of its {100} planes, it is useful to label the KS variants with a notation that specifies the Bain variant. Returning to figure 1, the three martensite variants that are associated with the $[1\bar{1}0]_\gamma$ direction in the $(111)_\gamma||(011)_\alpha$ plane (two KS, one NW), can be shown to be examples of the three different Bain variants. Arbitrarily choosing axes *X*, *Y* and *Z* for the Bain axes, we label them *K1X*, *K2Y* and *NZ*. Moving around the triangle of close-packed directions in the $(111)_\gamma||(011)_\alpha$ plane, there are a total of six KS variants, two representatives of each of the three Bain variants, and three NW variants, one from each of the Bain variants. The nine variants are systematically labeled in table 1 in the notation that emphasizes the Bain variant. The Maki notation for the KS variants also included.

The concept of a Bain variant and the nature of its transformation strain make it relatively simple to describe the complex structure of lath martensitic steels.

2.2. The 'classic' microstructure of lath martensitic steel

The complex mesostructure that develops on transforming a large-grained prior austenite grain in a prototypical lath martensitic steel is illustrated in figure 3, taken from Maki [6]. The prior austenite grains are divided into 'packets' that are subdivided into 'blocks' of martensite laths. Particularly when the structure is coarse-grained, as in the figure, the blocks are often found to contain two interleaved KS variants in the specific pairs, V1–V4, V2–V5 and V3–V6. When the blocks are interleaved pairs then the packets ordinarily contain three crystallographically distinct blocks, one made from each pair.

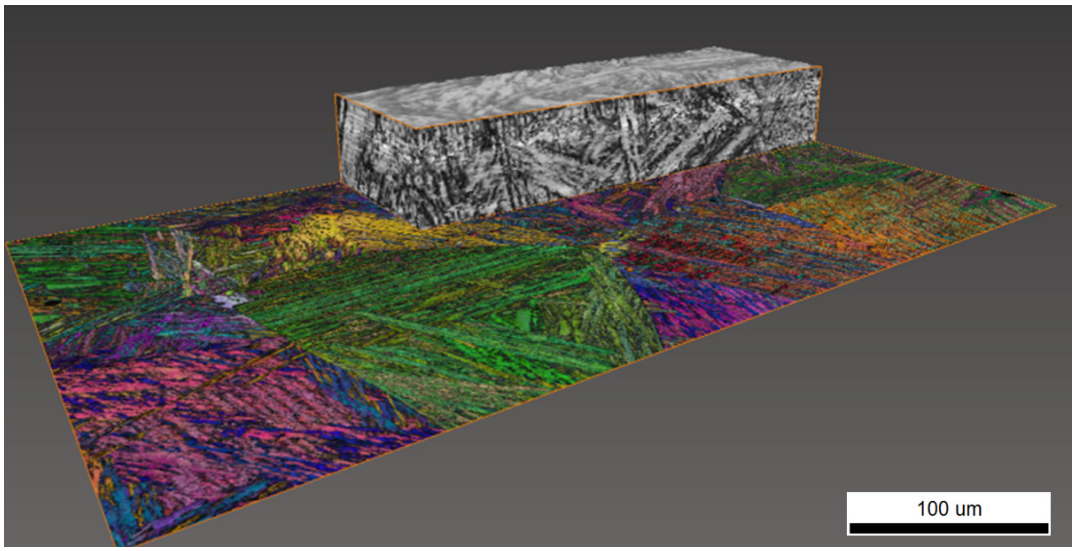

Figure 4. The microstructure of 9Ni steel, annealed and quenched from coarse-grained austenite. The colored image on the bottom plane is an EBSD IPF map, and the black and white contrast of the 3D section is from optical microscopy after a 1% Nital etch.

Examining the transformation strains (equation (1)) makes it clear why the structure described by Maki and co-workers [6–8] tends to appear [10]. In this structure, martensite blocks are composed of the two KS variants that share the same Bain axis; the diagonal elements of the transformation strain are the same, but the off-diagonal elements largely cancel. An equal mixture of these has a net transformation strain that is almost a simple tetragonal strain. Packets are ideally composed of three such blocks, one for each Bain variant. When the three Bain variants are present in equal fractions, the net transformation strain is almost a simple dilation, that is, the transformation strain that is most easily accommodated in a constrained polygranular matrix. A martensite packet is, then, a set of blocks that share the same one of the four independent {111} planes of the parent austenite.

We can, therefore, describe the 'classic' lath martensite structure as follows. Each prior austenite grain is subdivided into packets whose close-packed planes parallel the same $\{111\}_\gamma$ austenite reference plane. There are four distinguishable packets. Each of these packets is subdivided into 'blocks' of laths that have the same Bain variant. The laths in the block will preferentially be interleaved examples of the two KS variants in the packet that have the same Bain variant. The packet preferentially contains equal fractions of the three Bain blocks, since this arrangement minimizes the elastic energy.

Structures as 'simple' as this 'classic' structure described by Maki and co-workers [6–8] are rare. More complex arrangements appear as the composition is varied or the prior austenite grain size is refined. As the prior austenite grain size is refined, only one or two blocks appear in the grain; adjacent grains apparently adopt variants that balance the transformation stress, but the polygranular accommodation mechanisms have not been studied in detail.

2.3. The microstructure of quenched 9Ni steel

To explore the applicability of the 'classic' model of lath martensite to more complex, high-alloy steels we investigated the microstructure of a conventional 9Ni steel. The research sample was provided by POSCO, and had the composition, Fe–9Ni–0.5Mn–0.05C (wt%). It was annealed to produce a prior austenite grain size $>100\ \mu$m, then quenched to produce a homogeneous microstructure of dislocated lath martensite.

The microstructure of the sample is presented in figure 4, which shows a magnified image of a small volume of the material superimposed on an EBSD map of the basal plane of the block. The image of the block was created by serial sectioning, using a device (Genus_3D) developed by one of us (Adachi). Note the visual irregularity of the lath structure, in contrast to the relative simplicity of the structures studied by Maki and co-workers [6–8].

Figure 5 shows a section through the microstructure that includes several prior austenite grains. The left-hand figure is an EBSD map that makes it relatively easy to distinguish the various prior austenite grains, four of which are labeled.

We are first interested in the packet structure of these grains. As discussed above, a packet is a neighboring set of laths that share a common {110} plane. The three figures on the right in figure 5 show the prior austenite grains 1, 2 and 3, with the EBSD data used to highlight those regions that share a common close-packed plane. Each prior austenite grain (and, in fact, all of those we have examined in this coarse-grained sample) contains packets whose close-packed planes lie in four distinct orientations, corresponding to the four possible packet orientations (that is, the four possible orientations of the close-packed planes of the parent austenite grain). The four packets are tinted orange, yellow, purple and gray in the figure.

Each of the prior austenite grains contains all four distinct packets. There are, in fact, spatially distinct areas of the same packet in each of the grains, which suggests that the large prior

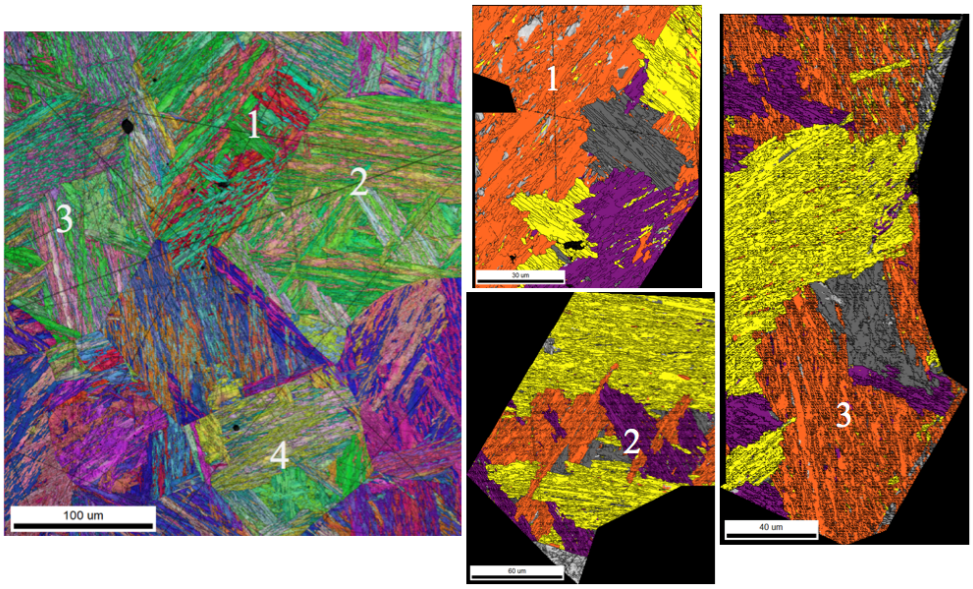

Figure 5. EBSD analysis showing the packet structure of three prior austenite grains. The four distinct packets are colored yellow, orange, purple and gray. Each grain contains all four distinct packets. The length scales of images 1, 2 and 3 are 30, 60 and 40 μm, respectively.

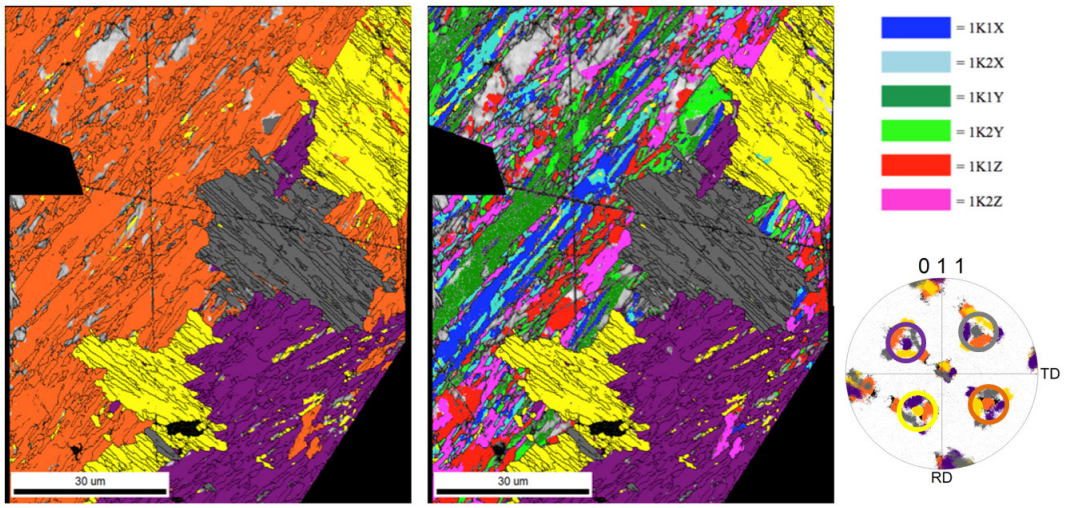

Figure 6. The lath and block structure of the 'orange' packet (packet 1) with laths colored by Bain variant, according to the table and (011) pole figure at the right. The light gray areas are those that did not yield good EBSD data.

austenite grains are subdivided into more than four packets, with multiple examples of at least some of them. Of course, it is not possible to establish that from a two-dimensional section, since packets may be irregular in shape and intersect the plane of the section in more than one area.

We now turn to examine the lath and block structure within the packet, arbitrarily focusing on prior austenite grain 1. The left-hand map in figure 6 gives a magnified view of the packet structure in grain 1. In the right-hand map the 'orange' packet, arbitrary labeled packet 1, is re-mapped to show its lath and block structure. Each lath is colored according to its Bain variant, using the color scheme shown at the right. Note that all six variants appear in the packet. The packet does contain long, reasonably well-defined blocks in which the two variants with the same Bain axis are interleaved. These blocks tend to be 5–10 μm in thickness. There are also less regular regions where different Bain variants are intermixed, leading to a very fine block size. Note also the small areas at the lower right where examples of this packet have intruded into the 'purple' packet.

The right-hand map in figure 7 shows the lath and block structure of the 'yellow' packet (packet 2), with the laths colored according to variant, according to the legend on the right. The packet appears in two disconnected areas, and there are narrow streaks of this packet orientation within the 'purple' packet. Again, all six variants are present, and are found in each of the large areas, though they are not uniformly distributed. Both areas contain reasonably well-defined blocks in which the two variants that share a Bain axis are interleaved, though other regions show more chaotic variant mixtures.

These results show that the microstructure of 9Ni steel with a coarse prior austenite grain size tends to adopt the

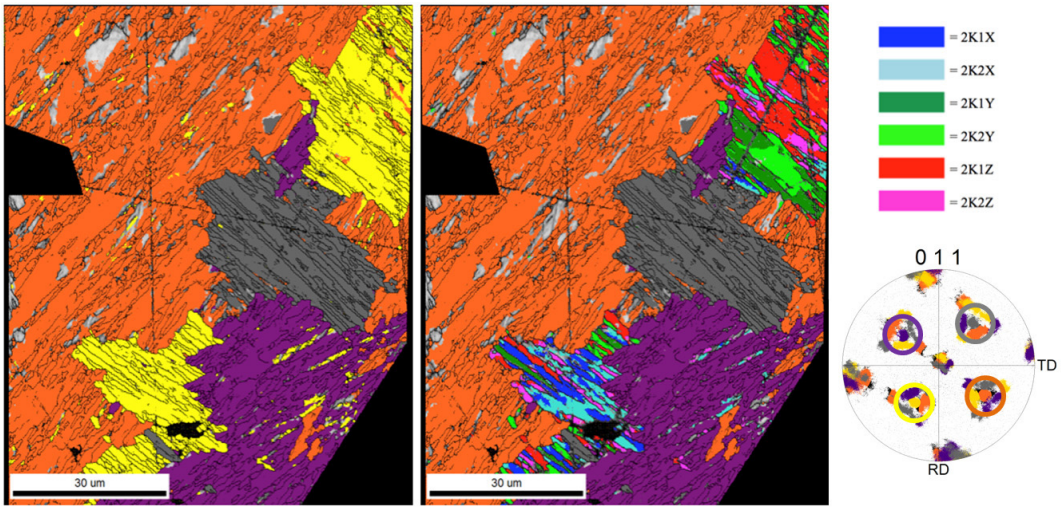

Figure 7. The lath and block structure of the 'yellow' packet (packet 2) with laths colored by Bain variant, according to the table and (011) pole figure at the right. The light gray areas are those that did not yield good EBSD data.

'classic' structures: prior austenite grains are subdivided into packets with all of the four possible packets represented, and each packet contains all six of the pertinent KS variants. It is common to find blocks of 5–10 μm thickness that traverse the packet. However, there are also areas in which individual laths are assembled in a more chaotic arrangements, breaking up the long-range pattern.

3. The influence of the microstructure on cleavage

One of the most important characteristics of the microstructure is its influence on the ductile–brittle transition of the steel. In clean, lath martensitic steels the brittle fracture mode is transgranular cleavage, so we need to understand the role of the microstructure in inhibiting cleavage. As is well known, cleavage is best inhibited by refining the effective grain size to introduce barriers to crack propagation. Since iron cleaves on {100} planes, and since the orientation of the {100} planes necessarily changes at boundaries between different Bain variants (figure 2), the effective grain size for cleavage is expected to be the block size.

An apparent example of this process is shown in figure 8, which is a profile scanning electron microscopy (SEM) fractograph of brittle fracture in an Fe–12Ni–0.25Ti alloy broken in impact at 77 K. This steel, which appeared to have had a large block size, shows planar fracture on a common {100} plane that crosses many laths. The central cleavage facet terminates at a prior austenite grain boundary on its right, but ends in a right-angle turn on its left, then branches to propagate both vertically into the steel and horizontally back along the dominant fracture plane. The right-angle turn in the crack path is particularly puzzling.

We hence fractured and analyzed a coarse-grained 9Ni steel sample like that above in an attempt to clarify this behavior.

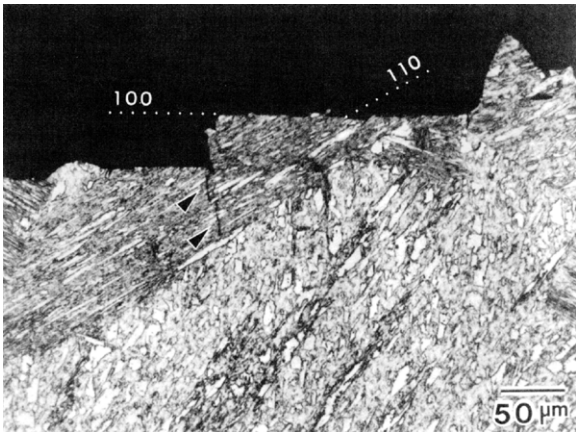

Figure 8. Cleavage in lath martensitic steel (Fe–12Ni–0.25Ti). This secondary electron SEM image of an etched sample shows crack propagation across many laths on common {100} cleavage planes [11].

3.1. Cleavage in coarse-grained 9Ni steel

Figure 9 shows a profile fractograph of brittle fracture in the coarse-grained 9Ni steel under study here, where the brittle fracture was achieved by breaking a fatigue pre-cracked Charpy specimen in impact at 77 K. The fracture surface was then coated with electroless Ni to protect it during polishing.

The upper fractograph shows the crack moving in from the left across a low-angle prior austenite grain boundary. The crack then executes four abrupt right-angle turns, similar to that seen in figure 8, before leaving the field of view to the right.

A likely reason for this jagged growth pattern becomes clear when we re-plot the EBSD data to show the lath structure of the central grain. The propagating fracture cleaves the red, Y-block, but deflects on contacting the green, X-block. It resumes its progress, possibly passing over the top of the first green block before being deflected again at the second green

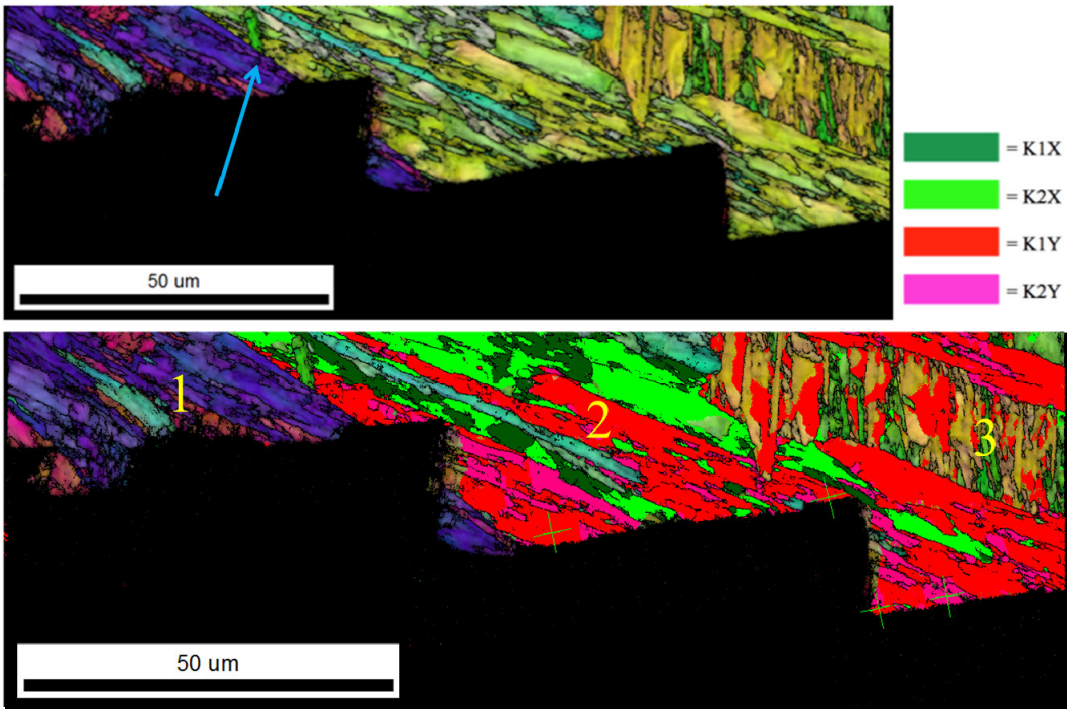

Figure 9. Profile fractograph of local cleavage fracture in 9Ni steel. The brittle crack enters from the left across a low-angle prior austenite grain boundary (blue arrow), then executes four abrupt right-angle turns before exiting to the right. The lower figure shows the lath structure of the central grain.

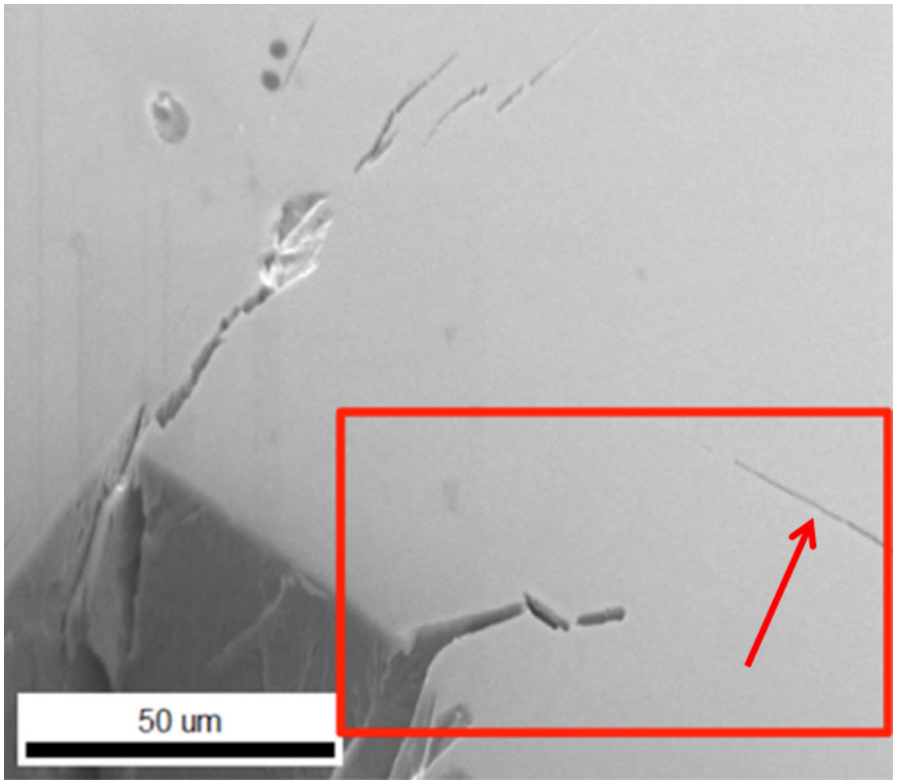

Figure 10. Secondary electron SEM image shows that a facet in the fracture surface of the 9Ni specimen produces a jagged secondary crack within the outlined box. A second, straight crack is also in the box, above the fracture surface.

block. It defects far enough to pass over the top of this block and moves out of the picture.

The cleavage crack deflects at the block boundaries. Since the {100} cleavage planes within a given block are at right angles, the path across a given block is jagged, with right-angle turns.

A second of the many interesting features on this fracture surface is shown in figure 10. Focusing on the region

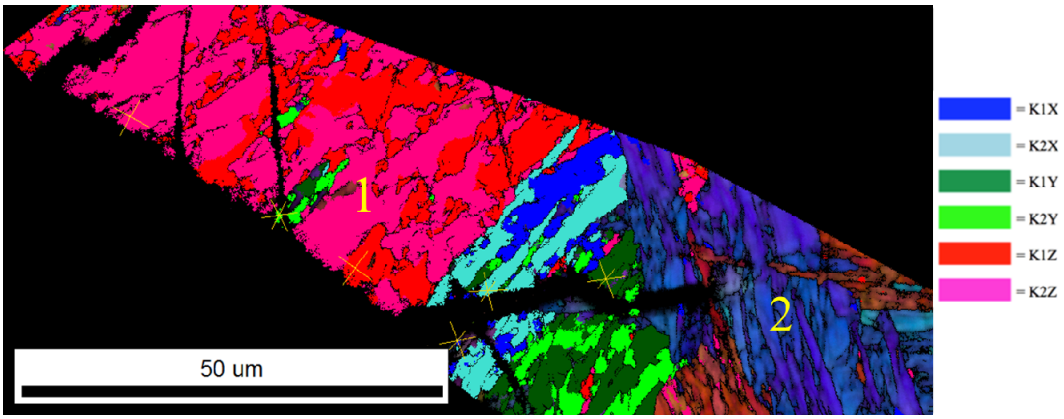

Figure 11. EBSD map showing the block structure near the jagged secondary crack in figure 10. The laths are colored according to the key at right. The off-color area to the right is a second packet in the same prior austenite grain. The boundary along the top is a prior austenite grain boundary.

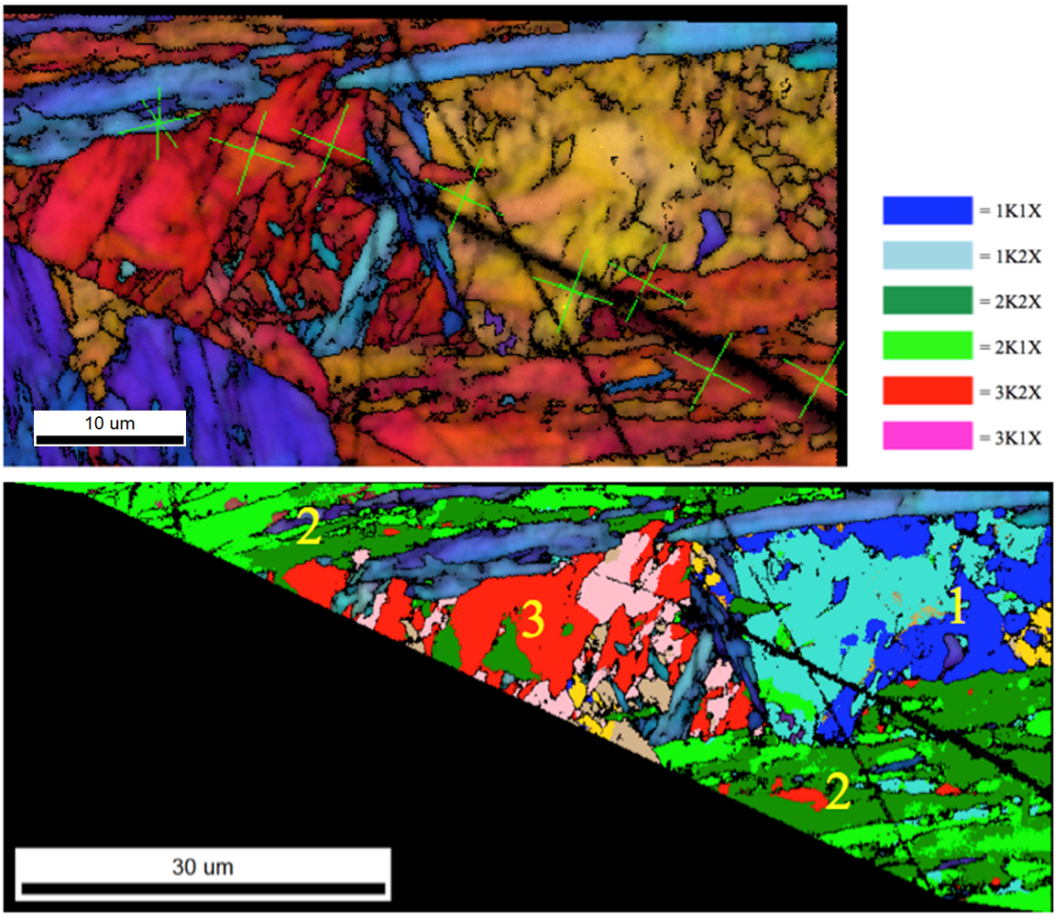

Figure 12. EBSD maps of the region containing the straight subsurface crack shown in figure 10. The lower figure maps the most prominant blocks, colored according to the legend at right. The blocks from three different packets, all with the same Bain axis. The dull blue feature is an intrusion from a distinct block with a different Bain axis.

outlined in red, we see a facet on the primary fracture surface that produces a jagged secondary crack that penetrates into the material. There is a second crack in the box, a nearly straight crack that parallels the fracture surface a bit above it.

Figure 11 is an EBSD map of the jagged secondary crack within the box in figure 10 and the primary fracture surface leading to it. The map is terminated on the top at a prior austenite grain boundary. The structure in the adjoining prior austenite grain is mapped in figure 12.

The flat cleavage fracture on the primary fracture surface in figure 11 is the cleavage of a single, large block. At its right edge this crack encounters a block boundary and bifurcates, creating a roughness in the primary crack path and sending a

secondary crack into the 'blue' block. It can be shown that the crack path through the blue block is consistent with cleavage on a {100} plane. The crack deflects at the boundary between the blue and 'green' blocks, cleaving the green block on a path consistent with {100} cleavage. The secondary crack jogs again at the packet boundary between packets 1 and 2, and blunts out after progressing a short distance into that packet.

Now consider the straight subsurface crack that appears in the box in figure 10. Given that straight cracks are associated with the cleavage of single blocks, it is tempting to assume that this crack is associated with a single, large block. The upper EBSD map in figure 12 shows that this is not the case. The crack wends its way through three blocky features, yet remains straight.

The lower map in figure 12 provides an explanation for the straight crack path. The three blocky features are blocks that have the same Bain variant, but are crystallographically distinct since they are contained in three different packets. Since blocks from different packets that have the same Bain variant have nearly parallel {100} cleavage planes, the cleavage crack can easily propagate across the boundaries between them. The crack trace lies along a ⟨100⟩ direction as shown by the oriented ⟨100⟩ axes plotted in the upper figure. The dull blue features in the map are laths of a different Bain variant. If we assume the crack propagates from right to left, it appears to circumvent the first set of such laths (the laths are not fractured) but is stopped by the second set. The long line that intersects the crack is probably a slip line that disturbs the local crystallography.

4. Discussion and conclusion

While the microstructure of quenched 9Ni steel does appear more complicated than that of the low-carbon steels studied by Maki co-workers [6–8], it does contain the same basic features, which, we believe, can be properly called the 'classic' microstructure of dislocated lath martensite. The prior austenite grains are divided into packets, and all those examined contain examples of all four of the crystallographically distinct packets. The packets contain laths with all six of the possible KS-relations for the packet. These tend to be organized into well-defined blocks in which the two KS variants that have the same Bain axis are interleaved. The blocks tend to be 5–10 μm in width, and traverse the packet, which varies from 10–100 μm in size in the example studied here.

However, the classic block structure is imperfect. There are block-like features that contain fine-scaled mixtures of different Bain variants (effectively, a mixture of different nano-blocks), and there intrusions where the wrong Bain variant appears in a packet, or a feature from a different packet appears. Of course, since our map is a slice through the microstructure it is not yet possible to say whether these imperfections are intrusions, or simply sections through irregular boundaries between volumes whose microstructures are more regular.

A survey of the brittle fracture surface of a sample that was broken at 77 K shows the central role of blocks and their Bain variants in controlling cleavage fracture. Blocks have a strong tendency to cleave as a unit, and cleavage cracks branch or bifurcate when they encounter a boundary between blocks with different Bain axes. On the other hand, block boundaries that separate blocks with the same Bain axis, such as equivalent blocks from different packets, appear transparent to cleavage fracture.

We also note that the blocks that appear in the cleavage fracture surface tend to be larger than the typical blocks in the microstructure, and seem always to be almost perfect, classic blocks. This is an expected consequence of the fact that the cleavage crack is free to choose its path, and the preferred path will path through blocks that are large and well defined, since these have minimal resistance to cleavage.

The results of this work illustrate and confirm principles of steel metallurgy that has been widely accepted and used: the effective grain size for cleavage fracture in lath martensitic steel is coherence length for the {100} cleavage crack planes. In classic lath martensitic steels this effective grain size is the block size, with the caveat that superficially distinct blocks in adjacent packets may have the same Bain variant, and, hence, share a common cleavage plane. The control of the block size is the ultimate path to control the ductile–brittle transition in lath martensitic steels.

The extension of this principle to martensitic steels with other substructures, and to Bainitic and ferritic steels, is being explored.

Acknowledgment

This work was supported by the National Science Foundation under grant number DMR1006160.

References

[1] Morris J W Jr 2009 Stronger, tougher steels *Science* **320** 1022–23
[2] Morris J W Jr, Guo Z, Krenn C R and Kim Y H 2001 The limits of strength and toughness in Steel *ISIJ Int.* **41** 599–611
[3] Morris J W Jr 2011 On the ductile–brittle transition in lath martensitic steel *ISIJ Int.* **51** 1569–75
[4] Marder A R and Krauss G 1969 *Trans. ASM* **60** 651
[5] Maki T, Tsuzaki K and Tamura I 1980 *Trans. ISIJ* **20** 209
[6] Maki T 2007 Recent advances in understanding martensite in steel *Fundamentals of Martensite and Bainite toward Future Steels with High Performance* ed T Furuhara and K Tsuzaki (ISIJ) pp 1–10
[7] Furuhara T, Morito S and Maki T 2007 On the controlling factors of grain sizes in martensite and Bainite *Fundamentals of Martensite and Bainite toward Future Steels with High Performance* ed T Furuhara and K Tsuzaki (ISIJ) pp 51–5
[8] Morito S, Tanaka H, Konishi R, Furuhara T and Maki T 2003 *Acta Mater.* **51** 1789
[9] Guo Z, Lee C S and Morris J W Jr 2004 On coherent transformations in steel *Acta Mater.* **52** 5511–8
[10] Morris J W Jr 2008 Comments on the microstructure and properties of ultrafine grained steel *ISIJ Int.* **48** 1063–70
[11] Kim J I, Syn C K and Morris J W Jr 1983 Microstructural sources of toughness in QLT-treated 5.5Ni cryogenic steel *Metall. Trans.* **14A** 93